Simulating tornado-like flows

Gillmeier, Steffi; Sterling, Mark; Hemida, Hassan

DOI:
10.1007/s11012-019-01082-4

Simulating Tornado-Like Flows – the Effect of the Simulator's Geometry

S. Gillmeier[1], M. Sterling[2], H. Hemida[3]

Department of Civil Engineering, School of Engineering, University of Birmingham, Edgbaston, Birmingham, B15 2TT, United Kingdom,
[1]stefaniegillmeier-wls@web.de, +31 402472414
[2]m.sterling@bham.ac.uk, [3]h.hemida@bham.ac.uk

ABSTRACT

Within the wind engineering community, a series of physical simulators of differing geometries have been used to investigate the flow-field of tornado-like vortices. This paper examines the influence that the geometry of a simulator can have on the generated flow field. Surface pressure and velocity data have been measured for two swirl ratios (S = 0.30 and S = 0.69) in two different simulators of different scale and varying geometry. The results of this research suggest that far from being a mature research field, there are still many unresolved questions that need to be addressed before data obtained from such simulators can be used with confidence in practice.

Keywords: Tornado-like vortex; Physical simulation; Simulator's design, Geometric parameters; Aspect ratio; Swirl ratio

1. INTRODUCTION

In recent years, increasing attention has been paid to the effects of non-stationary, non-synoptic winds with downbursts [1 - 3] and in particular tornadoes generating much significant research [4]. The latter is perhaps not too surprising when one considers the impact of such winds. For example, in 2011 North America experienced one of the most destructive tornado seasons with approximately 1600 tornado outbreaks reported and the total damage exceeding $28bn [5]. Considerable tornado losses also occur elsewhere around the world but not necessarily as frequently or to such an extent. The transient and violent nature of such events ensures that obtaining full-scale data at a resolution of interest to wind engineers is fraught with challenges. However, a number of excellent full-scale datasets have been obtained despite the aforementioned difficulties [6 – 14]. Unfortunately, the expense of obtaining such data and the spatial resolution of the flow field, i.e., at heights considerably larger than average low-rise buildings, prevent their general adoption in the wind engineering community, although this is slowly changing [15]. As a result, recourse is often made to physical and numerical simulations, with the former typically preceding the latter.

Hence, a variety of large (> 10m in diameter), medium (~ 2m-5m) and small (< 1m) scale physical simulators purporting to generate tornado-like flow fields have been used to investigate a variety of tornado related issues [16 - 24]. The vast majority of these simulators embody the principles initially developed by Ward [16], i.e., a tornado-like wind is created by generating a circulation in the presence of a suction updraft. Surprisingly, relatively little has been reported concerning the geometry of such simulators, with most new simulators having a large degree of geometric similarity.

Davies-Jones [25] undertook a simple dimensional analysis of a Ward-type simulator and highlighted six non-dimensional parameters of potential importance. The following four define the geometry of the simulator:

$$2H_1/D_3 \equiv G_a \quad (1)$$

$$H_2/D_1 \equiv G_b \quad (2)$$

$$D_2/D_1 \equiv G_c \quad (3)$$

$$D_3/D_1 \equiv G_d \quad (4)$$

where H_1 and D_3 are the height of the convergence chamber and the diameter of the updraft hole, respectively. H_2 and D_1 are the height of the convection chamber and the diameter of the convergence chamber, and D_2 is the diameter of the convection chamber. Exact locations of the aforementioned geometric variables are also illustrated in figure 1. A factor of two was introduced in equation (1) because the ratio between convergence chamber height and updraft radius ($D_3/2$) is frequently referred to as the aspect ratio (Eq. 1). Notwithstanding this, of the parameters listed in equations (1 – 4), over the years the main geometric parameter which has tended to be kept constant as new simulators were constructed is the aspect ratio (Eq. 1). Intuitively, one would expect the aspect ratio to play a major role in governing the generated flow field [26]; however, whether it is appropriate to elevate this parameter (Eq. 1) over the others (Eq. 2 – 4) is debatable and is investigated below. It also needs to be mentioned that there are other parameters that have not been taken into account, such as the design or the number of guide vanes, which could potentially affect the generated vortex flow structure.

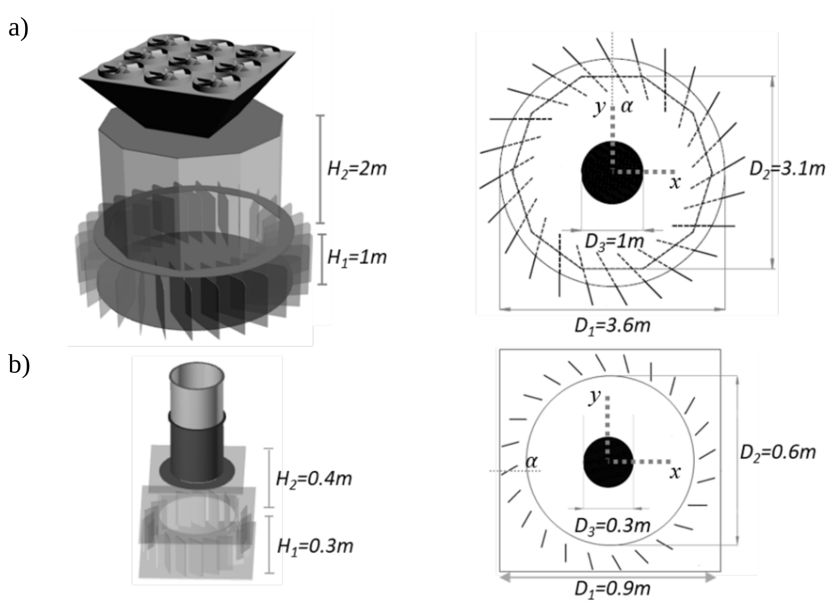

Fig. 1 An illustration of (a) the medium-scale (*M1*) and (b) the small-scale (*S1*) tornado-like vortex generator. H_1 and D_1 show the height and diameter of the convergence chamber, H_2 and D_2 show the height and diameter of the convection chamber and D_3 is the diameter of the updraft hole

Davies-Jones [25] acknowledged that the generated flow field is not simply a function of the geometric parameters but also a function of the volume flow rate through the simulator and the circulation at a certain location in the simulator. As a result, two additional non-dimensional parameters have received attention in the literature, i.e., the Reynolds number, *Re*, (Eq. 5) and a parameter which describes the effect of rotation on the flow field - the swirl ratio, *S*, (Eq. 6).

$$Re = \frac{2Q}{vD_3} \quad (5)$$

$$S = \frac{\tan(\alpha)}{2G_a} \quad (6)$$

where Q is the volume flow rate through the simulator, v is the kinematic viscosity of air and α is the guide vane angle relative to the radial velocity component.

Equation (6) is adopted in this research since it is the version which also has been widely used in Ward-type simulators and thus is helpful in undertaking relative comparisons between such simulators. It is acknowledged that such a definition raises a number of challenges, not least determining the equivalent full-scale value. Notwithstanding the issues that exist regarding the swirl ratio definition, the swirl ratio is generally accepted as an important parameter for tornado-like simulations and its effect on the generated vortex flow field has been investigated thoroughly [16 - 18, 21 - 25, 27 - 30].

Using a medium-scale simulator of fixed geometry and a small-scale simulator of variable geometry (Figure 1), this paper will investigate the influence of the simulators' varying geometric parameters on the simulation of tornado-like vortices. Section 2 of the paper outlines the experimental methodology, whereas section 3 presents results. Concluding remarks are given in section 4, which state that the approach (adopted by many) of 'simply' matching the aspect ratio and swirl ratio is insufficient to ensure flow field parity between vortices generated in different simulators.

In keeping with the work of previous authors, the investigation contained herein focuses on the behaviour of mean flow variables. However, it is acknowledged that tornadoes are non-stationary phenomenon and when simulated physically, a degree of non-stationarity often attributed to vortex wandering [e.g. 31] has been observed. Nevertheless, and as shown below, the importance of the geometric parameters in equations (1 - 4) can be observed through examining the mean flow parameters alone.

2. EXPERIMENTAL METHODOLOGY

2.1. Tornado-like vortex simulators

Figure 1 provides a schematic of the two Ward-type simulators used in the current research. The medium-scale simulator (*M1)* has a total height (H_1 + H_2) of 3m and a convergence chamber diameter of 3.6m. The small-scale simulator (*S1*) has a variable height between 0.4m – 0.7m (depending on setting, i.e., H_2 is variable) and a convergence chamber diameter of 0.9m. In both cases, angular momentum is introduced by guide vanes around the convergence chamber, which can be set to different angles. By changing the guide vane angle (α), the vorticity in the flow can be altered and different vortex structures can be generated. The geometric configurations of *M1* and *S1* result in an aspect ratio of G_a = 2 (Table 1a). It is noted that the aspect ratio is relatively large compared to the aspect ratios of simulators at Western University [22], Texas Tech University [19, 24] and Iowa State University (18). However, the tornado simulator at Purdue University [32] and the original Ward simulator [16] allow the simulation of tornado-like vortices with similar aspect ratios.

In order to investigate whether geometric parameters defined by equation (2 – 4) influence the generated tornado-like flow field, eight simulations have been undertaken (details of which are given in table 1), in order to evaluate:

T1) the effect of the simulator's geometry with constant aspect ratio and swirl ratio. In this case, the aspect ratio was fixed at 2 and the medium-scale (*M1*) and small-scale simulator (*S1*) were used.

T2) the effect that the convection chamber may have on the simulation. In this case, the convection chamber height (H_2) of the small-scale simulator was reduced from H_2 = 0.40m (*S1*) to H_2 = 0.25m (*S2*) to H_2 = 0.10m (*S3*), whilst all other geometric lengths were kept constant.

Geometric parameters listed in equations (1 – 4) are presented in table 1a for the medium-scale (*M1*) and the small-scale simulators (*S1 – S3*). In all cases, the flow fields of two swirl ratios (*S* = 0.30 and *S* = 0.69) are investigated. It is noted that for this research the swirl ratio is defined based on the guide vane angle (Eq. 3) but a detailed investigation regarding the swirl ratio and its alternative definitions is presented in section 3.1.3. Over the small range of the Reynolds numbers investigated (Table 1b), no Reynolds number dependency was found and as such is not considered further.

Table 1: Overview of non-dimensional geometric (a) and dynamic (b) parameters for the simulations undertaken

a)	G_a	G_b	G_c	G_d
M1	*2*	*0.56*	*0.86*	*0.28*
S1	*2*	*0.44*	*0.67*	*0.33*
S2	*2*	*0.27*	*0.67*	*0.33*
S3	*2*	*0.11*	*0.67*	*0.33*

b)	$Re \cdot 10^5$	
	S = 0.30	*S = 0.69*
M1	*10.1*	*9.1*
S1	*2.9*	*2.4*
S2	*2.6*	*2.2*
S3	*2.7*	*2.6*

2.2. Normalisation

Circumferential (u_θ), radial (u_r) and vertical (u_z) velocity components are normalised by a reference wind speed (u_{ref}) which is based on the volume flow rate (Q) measured across the updraft diameter D_3 of the simulators divided by the corresponding area of the updraft. Surface pressures (p) of corresponding simulations are normalised by the corresponding dynamic pressure (p_{ref}) which is based on (u_{ref}). Radial and vertical distances are normalised by the updraft diameter (D_3) and the convergence chamber height (H_1), respectively. Table 2 provides a list of relevant parameters required for the normalisation of the simulations conducted in *M1*, *S1*, *S2* and *S3* for S = 0.30 and S = 0.69.

Table 2: Volume flow rate, reference wind speed and reference pressure for the normalisation of results obtained in *M1*, *S1*, *S2* and *S3* for S = 0.30 and S = 0.69

	Q [m³/s]		$u_{ref} = 4Q / (\pi D_3^2)$ [m/s]		$p_{ref} = ½ \rho u_{ref}^2$ [Nm⁻²]	
	S = 0.30	S = 0.69	S = 0.30	S = 0.69	S = 0.30	S = 0.69
M1	7.6	6.9	9.6	8.7	55.3	45.4
S1	0.7	0.6	9.1	7.7	49.7	35.6
S2	0.6	0.5	8.3	7.1	41.3	30.2
S3	0.6	0.6	8.6	8.4	44.4	42.3

2.3. Measurement setup and data quality

The pressure data were measured on the ground plane along two mutually perpendicular lines denoted as x and y (Figure 1) every 0.01s for a period of 60 seconds using a Multi-Channel-Pressure-System manufactured by Solution for Research Ltd. Surface pressure taps are distributed along these lines with a spacing of 0.01m and 0.05m from the simulator's centre up to a distance of 0.15m and 0.75m for the small-scale simulators (*S1* – *S3*) and the medium-scale simulator (*M1*), respectively.

Point velocity measurements were obtained every 0.01s for a period of 80 seconds using a Cobra Probe (TFI instrumentation – Series 100 Cobra Probe) which was mounted to a two-axis traverse system inside the simulators. This traverse system enabled the probe to be positioned with an accuracy of $\pm$1mm at nine heights (z) above the simulator's surface (0.01m, 0.03m, 0.05m, 0.07m, 0.10m, 0.13m, 0.15m, 0.17cm and 0.20m) in the small-scale simulators (*S1* – *S3*) and nine heights above the simulator's surface (0.01m, 0.05m, 0.10m, 0.15m, 0.20m, 0.25m, 0.30m, 0.40m, 0.50m) in the medium-scale simulator (*M1*). The corresponding radial spacing of measurement positions from the centre of each convergence chamber up to a distance of 0.18m (small simulator) and 0.60m (medium simulator) was 0.010m and 0.025m, respectively. Whilst the Cobra Probe was supported by a relatively small traverse system, every effort was made to minimise its impact, with the main supporting section being located at a distance greater than the corresponding convergence chamber height from the measurement location. The actual size of the traverse system in *M1* and *S1* was ~10^3 smaller than the size of the convergence chambers. However, it is acknowledged that there could be an impact on the flow (similar to most systems in boundary layer wind tunnels). In an attempt to quantify the potential influence of the system, a series of pressure measurements were undertaken for a variety of swirl ratios with and without the system in place. No noticeable effect was observed on the measured data.

In order to evaluate potential differences in the simulations, it is important to account for experimental uncertainties. The experimental uncertainty is a combination of uncertainties due to measuring a finite time series (statistical uncertainty), operator error such as probe and guide vane angle positioning (repeatability) and the uncertainty of the measurement device itself. A detailed explanation of different uncertainties for measurements conducted in *M1* can be found in Gillmeier et al. [23]. A similar methodology was followed for velocity and surface pressure measurements in *S1 – S3* and for the sake of clarity are briefly outlined below.

In this research, pressure transducers (*HCLA12X5DB*) with a typical uncertainty of ± 5 Nm^{-2} were used. The Cobra Probe is accurate to within ± 0.5 m/s for the velocity vector up to a turbulence intensity of ~30%. Therefore, positions with a turbulence intensity greater than 30% are excluded from the comparison analysis. Furthermore, the Cobra Probe can measure velocity data greater than 2 m/s within a cone of influence of $\pm 45°$. These limitations can have a direct influence on the measured data. For example, if the recorded data quality (defined as the percentage of velocity samples of a measured time series which are greater than 2 m/s and have an angle of attack less than $\pm 45°$) is less than 100%, then this can introduce a bias in the calculated velocity vector – the lower the data quality the greater the potential bias. To minimize the bias in time averaged velocities, only those positions with a data quality of greater than 80% were accepted for the comparison analysis. This threshold is assumed to provide a suitable compromise between data quality and quantity.

In order to assess the statistical uncertainty, convergence tests were conducted for 600 seconds at the core radius (R) of corresponding simulations. (i.e., at the radial distance (r) and height (z) at which the overall maximum circumferential velocity component occurs). For surface pressures, convergence tests were conducted at the centre of the simulators. It was observed that after 60 seconds, the uncertainty in determining time-averaged surface pressures decreased to below $\pm 6\%$ and $\pm 1\%$ of the time-average obtained after 600 seconds in all simulations for S = 0.30 and S = 0.69, respectively. For velocity measurements, an averaging time of 80 seconds allows to determine circumferential and vertical velocities with an uncertainty below $\pm 2\%$ for all simulations. Statistical uncertainties of radial velocity components are approximately $\pm 3\%$ and $\pm 0.5\%$ for S = 0.30 and S = 0.69, for all simulations.

The measurement repeatability is analysed in form of a distribution of all possible differences of repetition measurement datasets. Surface pressure and velocity measurements were repeated five times along the radial profile at the surface and at a height of z = 0.01m for each swirl ratio. The standard deviation (σ) of the corresponding distributions was chosen as a representative measure to evaluate the repeatability (Table 3). It was found that the repeatability is swirl ratio dependent. Furthermore, for S = 0.30 the repeatability of surface pressure measurements seems to be dependent on the radial distance. For that reason, a repeatability dependent on r is introduced for the surface pressures obtained with S = 0.30 since a uniform value would highly underestimate the repeatability of measurement positions close to the vortex centre, and highly overestimate the repeatability for positions further away from the vortex centre. Therefore, in table 3, the repeatability of surface pressure measurements for the lowest swirl ratio is given for normalised radial locations of $r/D_3 \leq$ 0.1 and larger than 0.1.

Table 3: Repetition uncertainties for velocity components (a) and surface pressures (b) in *M1, S1, S2, S3* and for S = 0.30 and S = 0.69

a)

	u_θ/u_{ref} [-]	u_r/u_{ref} [-]	u_z/u_{ref} [-]	u_θ/u_{ref} [-]	u_r/u_{ref} [-]	u_z/u_{ref} [-]
	S = 0.30			*S = 0.69*		
M1	±*0.05*	±*0.06*	±*0.02*	±*0.04*	±*0.03*	±*0.01*
S1	±*0.07*	±*0.06*	±*0.03*	±*0.02*	±*0.03*	±*0.02*
S2	±*0.03*	±*0.10*	±*0.03*	±*0.05*	±*0.02*	±*0.02*
S3	±*0.02*	±*0.05*	±*0.02*	±*0.04*	±*0.07*	±*0.02*

b)

	$p/p_{ref_{(r/D3 \le 0.1)}}$ [-]	$p/p_{ref_{(r/D3 > 0.1)}}$ [-]	p/p_{ref} [-]
	S = 0.30		*S = 0.69*
M1	±*0.31*	±*0.07*	±*0.12*
S1	±*0.17*	±*0.07*	±*0.07*
S2	±*0.49*	±*0.16*	±*0.11*
S3	±*0.14*	±*0.06*	±*0.06*

In what follows, the measurement repeatability is used to quantify the experimental uncertainty since statistical and device uncertainties are assumed to be reflected within the uncertainty given by the repeatability. Therefore, the repeatability is assumed to provide a reasonable estimate for the experimental uncertainties.

3. RESULTS

To assess the influence of the simulator's geometry and corresponding geometric changes, in this section, flow field and surface pressure data obtained in *M1*, *S1*, *S2*, and *S3* are compared. The very nature of the experimental equipment and the scale of the generator prevents in some cases a detailed knowledge of the flow structure across the entire flow field. As a result, for some simulations presented below, the complex flow structure inside the vortex could not be captured in detail. However, sufficient data has been gathered which we postulate enables a relative comparison of flow fields and as a result provides an insight into the question at hand, i.e., does the geometry of the simulator influence the generated tornado-like flow field?

3.1. SIMULATIONS IN S1 AND M1

3.1.1. The flow fields

The 3-D mean velocity fields obtained in *S1* and *M1* for $S = 0.30$ and $S = 0.69$ are shown in figure 2.

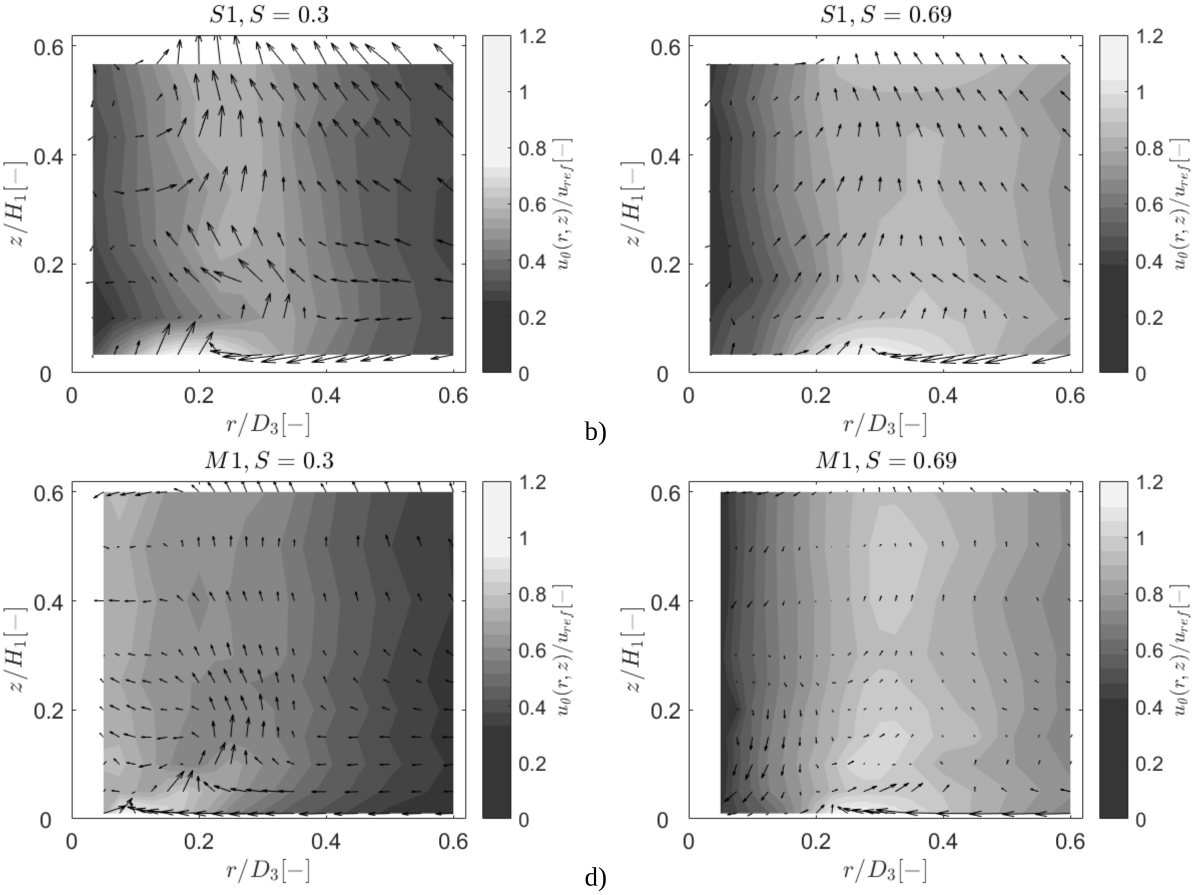

Fig. 2 3-D mean velocity fields in *S1* and *M1* for *S = 0.30* and *S = 0.69*. The normalised circumferential velocity component is shown as contour and the 2-D vector field indicates the vector based on the radial and vertical velocity component

Figure 2 highlights a number of similarities, e.g., for both swirl ratios in *S1* and *M1*, the circumferential velocity component increases towards the vortex core radius and reaches the overall maximum close to the surface. In *S1*, for the lower swirl ratio (S = 0.30) the core radius of the simulated vortex is approximately defined at r/D_3 = 0.2, whereas for the same swirl ratio in *M1*, the vortex core radius extends to about r/D_3 = 0.1. For the larger swirl ratio (S = 0.69) the core radius increases to a normalised radial distance equal to approximately r/D_3 = 0.3 in both simulators. Figure 2 also reveals a strong radial inflow close to the simulator's surface up to the position where the corresponding overall maximum of the circumferential velocity component occurs. This flow behaviour was found to be present for both swirl ratios in both simulators.

Figure 2a shows that for S = 0.30 in *S1*, radial inflow is dominant inside the vortex core (i.e., $r/D_3 \leq 0.2$) and for normalised heights $z/H_1 < 0.3$. This finding, in combination with the radial outflow from the vortex centre at larger normalised heights ($z/H_1 > 0.3$) could lead to the conclusion of a flow structure similar to what might be expected for a 'vortex breakdown'. For the larger swirl ratio, a central outflow is observed for all heights in *S1* (Figure 2b). This is a flow behaviour similar to what is expected in a two-celled vortex structure.

The 3-D velocity field obtained in the medium simulator (*M1*) for S = 0.30 shows tentative evidence to suggest the presence of a counter-clockwise rotating cell near the surface close to the vortex centre covering a normalised area of approximately 0.1 x 0.1(Figure 2c). At greater heights, the vortex core is dominated by radial inflow and updraft, which turns into a downdraft at a normalised height of z/H_1 = 0.6, potentially suggesting a second counter-clockwise rotating cell in the vortex core at greater heights. With increasing swirl ratio (S = 0.69) in *M1*, a downdraft is detected in the vortex centre, which seems to feed into the radial outflow observed at the lowest height (Figure 2d). This describes a flow structure, which might be expected for a two-celled vortex. However, the central downdraft is directed slightly towards the simulator's centre, which in general is not expected in a 'typical' two-celled vortex; however, was also observed by Haan et al. [18] for a high swirl ratio.

3.1.2. The effect of the simulator's geometry on the flow field (*T1*)

In order to allow a representative comparison between flow fields simulated in *S1* and *M1*, flow characteristics at equal relative heights (z/H_1) are compared in this section. Table 4 illustrates that for each comparison two heights are determined (z_1 and z_2) which lead to the same relative heights in simulator *S1* and *M1*.

Figure 3 illustrates the radial profile of circumferential (a), radial (b) and vertical (c) velocity components obtained in *S1* and *M1* for S = 0.30 (1) and S = 0.69 (2) at corresponding relative heights given in table 4.

Table 4: Absolute (z) and relative (z/H_1) heights for the comparison of flow fields simulated *S1* and *M1* for S = 0.30 and S = 0.69

	S1	*M1*
z_1 [m]	*0.03*	*0.10*
z_2 [m]	*0.15*	*0.50*
z_1/H_1	*0.1*	*0.1*
z_2/H_1	*0.5*	*0.5*

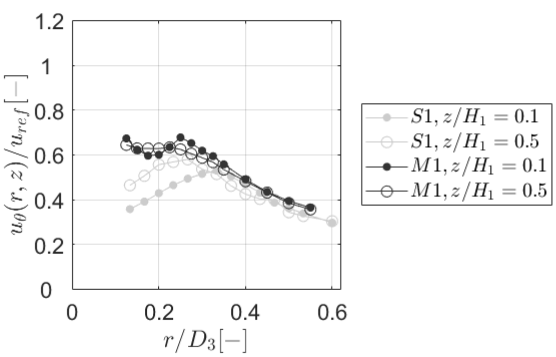

a1)

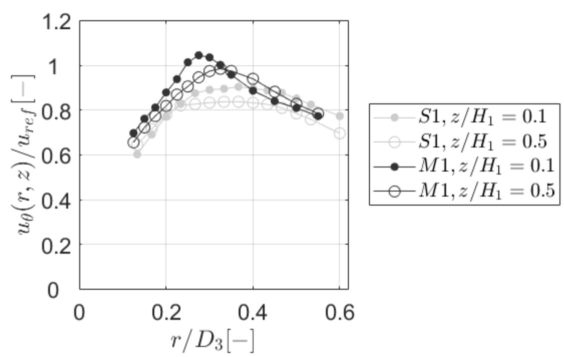

a2)

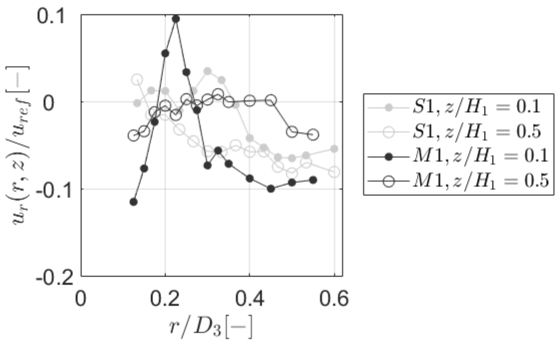

b1)

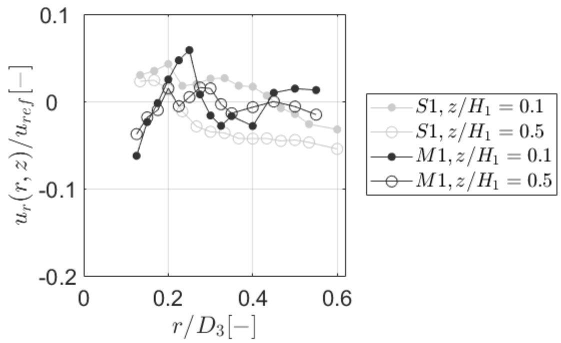

b2)

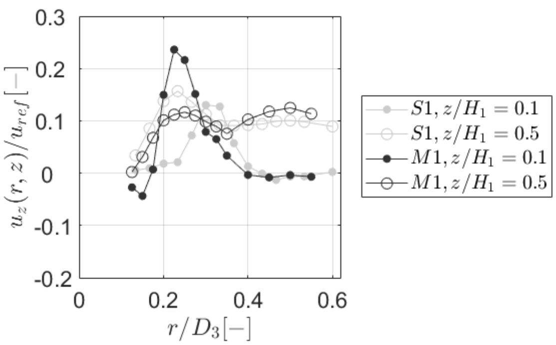

c1)

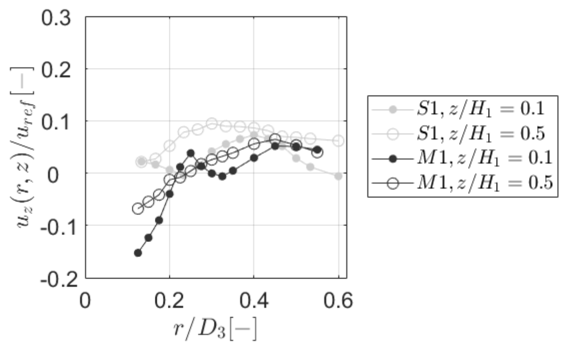

c2)

Fig. 3 Radial profile of mean circumferential (a), radial (b) and vertical (c) velocity components obtained in *S1* and *M1* for S = 0.30 (1) and S = 0.69 (2) at corresponding relative heights (z/H_1)

Figure 3 shows differences larger than the corresponding experimental uncertainty (defined in table 3) between the flow fields obtained in *S1* and *M1* for both swirl ratios. In what follows, differences between velocity components obtained in different simulators will be presented in the following form: ($\delta u_x = \left|(u_x(r,z)/u_{ref})_{S1} - (u_x(r,z)/u_{ref})_{M1}\right|$).

Circumferential velocity components obtained in *S1* and *M1* for the smaller swirl ratio (S = 0.30) differ significantly at radial distances < 0.3 r/D_3 for both heights investigated (Figure 3a1). In this flow region, circumferential velocity components were found to be larger by approximately $0.2\delta u_\theta$ in *M1* compared to *S1*. Figure 3b1 reveals differences between the radial profile of radial velocity components in *S1* and *M1*. For the lowest height investigated, differences of approximately $0.1\delta u_r$ can be observed. Those differences originate from the radial inflow, which extends further in *M1* compared to *S1*. At the larger relative height (z/H_1 = 0.5) and at a radial distance of r/D_3 = 0.1, a weak central outflow can be detected in *S1*, whereas radial inflow seems to dominate the flow field in *M1*. Vertical velocity components obtained in *M1* for S = 0.30 differ only at the lower height investigated (Figure 3c1). At this height (z/H_1 = 0.1) and at a radial distance of r/D_3 = 0.2, vertical velocities are found to be larger by $0.2\delta u_z$ in *M1* compared to *S1*. This is the case because the maximum vertical updraft occurs at smaller radial distances in *M1* compared to *S1*.

For S = 0.69, circumferential velocity components reveal differences of up to $0.2\delta u_\theta$ at a flow region around the vortex core ($0.2 < r/D_3 < 0.4$) for both heights investigated (Figure 3a2). The region of maximum circumferential velocities is not as well defined in *S1* compared to *M1*, which leads to a relatively uniform distribution of circumferential velocities around the vortex core in *S1*. Differences observed between radial velocities in *S1* and *M1* are small and therefore, are largely masked by the experimental uncertainty (Figure3b2). Only at the lowest height investigated (z/H_1 = 0.1), the weak radial inflow present in *M1* and the weak radial outflow observed in *S1* causes differences larger than the measurement uncertainty of approximately $0.1\delta u_r$. Largest differences between vertical velocity components in *S1* and *M1* are obtained at radial distances < $0.2r/D_3$ for both heights investigated (Figure 3c2). In this region, the flow field at the lowest height (z/H_1 = 0.1) differs by about $0.15\delta u_z$, whereas differences in the larger height are $0.05\delta u_z$. Observed differences can be explained by the downdraft captured in *M1* which extends to approximately r/D_3 = 0.2, whereas in *S1* the downdraft occurs at radial distances closer to the simulator's centre.

When highlighting those differences between flow fields simulated in different simulators but aspect ratio and swirl ratio parity, the question arises, whether, the swirl ratio defined based on the guide vane angle (Eq. 6) might not be a representative parameter to determine the similarity of flow characteristics. In order to address this question in more detail the following section analyses swirl ratios defined at different locations in the generated flow fields.

3.1.3. The swirl ratio of flow fields simulated in *S1* and *M1*

In this section, swirl ratios are calculated for the flow fields simulated in *S1* and *M1* using the following equations:

$$S_2 = \frac{\Gamma_{average\ (r=D_3/2)}\ D_3}{4Q} \tag{7}$$

$$with\ \Gamma_{average\ (r=D_3/2)} = \frac{1}{N}\sum_{i=1}^{N}\left(\Gamma_{(r=D_3/2)}\right)_i$$

$$S_3 = \frac{\Gamma_{(R)}\ D_3}{4Q} \tag{8}$$

$$S_4 = \frac{\Gamma_{(R)}\ R}{2Q} \tag{9}$$

Here, $\Gamma(r)$ is the circulation ($\Gamma(r) = 2\pi r u_\theta(r)$), N is the number of measurement heights in the corresponding simulator and i represents an individual measurement height.

The definition adopted in equation (7) is based on the height average of swirl ratios at $r = D_3/2$ and is identical to the swirl ratio used by Tang et al. [24]. Equation (8) is similar to the definition adopted by Refan and Hangan [22], whereas Haan et al. [18] introduced equation (9).

The difference between the definitions shown in equations (6 and 7) and equation (8) is that the length scale in the numerator of S_3 (Eq. 8) is not identical to the radial distance at which the circulation is estimated. Furthermore, it needs to be mentioned that the swirl ratio defined in equation (6) is the only swirl ratio (from those presented) that is independent from any direct velocity measurement and that swirl ratios defined by equations (7 – 9) are calculated based on parameters (such as Γ and R) which are dependent on parameters defined in equations (1 – 6).

An overview of corresponding swirl ratio values for the flow fields obtained in *S1* and *M1* is presented in table 5.

Table 5: Swirl ratios (S and S_2 – S_4) defined at different locations in the flow fields of *M1* and *S1*

a)

	Figure	S	S_2	S_3	S_4
S1	*2a*	*0.30*	*0.35*	*0.30*	*0.11*
M1	*2c*	*0.30*	*0.38*	*0.28*	*0.03*

b)

	Figure	S	S_2	S_3	S_4
S1	*2b*	*0.69*	*0.81*	*0.62*	*0.35*
M1	*2d*	*0.69*	*0.82*	*0.55*	*0.25*

Because of the forced aspect ratio and guide vane angle parity between both simulators, S is identical (Table 5a and 5b).

Table 5 illustrates that for both flow fields in both simulators, S_4 shows the lowest and S_2 the highest swirl ratio. The reason for this can be found in the numerators of equations (9 and 7). Since the circulation is proportional to the radial distance, S_2 and S_4 are proportional to the square of the radial distance. Consequently, S_4 is calculated at relatively small radial distances ($r = R$) and S_2 is calculated at relatively large radial distances ($r = D_3/2$). Since, S_3 is defined based on a combination of R and $D_3/2$ (Eq. 8) its value lies in-between the values obtained for S_2 and S_4 (Table 5).

In order to determine whether swirl ratio parity between flow fields simulated in *S1* and *M1* is given regardless of the adapted definition, the accuracy with which each swirl ratio can be determined needs to be quantified. For S (Eq. 6), a possible source of uncertainty is the accuracy with which the guide vane angle can be adjusted. For S_2 and S_3, the uncertainty is partly determined by the uncertainty of the circumferential velocity component. For S_4 the uncertainty of R is an additional limitation for the swirl ratio's accuracy. As a result of those uncertainties, the swirl ratios presented in equations (6 – 8) are only accurate to one decimal place. The accuracy of the swirl ratio defined in equation (9) is even lower. With this additional information, table 5 reveals that swirl ratio parity is given for both flow fields investigated in *S1* and *M1*, regardless of which definition for the swirl ratio is used. This finding suggests that the geometric differences of both simulators are the cause of observed differences between the flow fields.

Additionally, it is noted that swirl ratios presented here are calculated based on time-averaged quantities of the circulation and the flow rate and therefore, conclusions can only be drawn with respect to the time-averaged flow behaviour. The instantaneous flow field of two vortices of similar swirl ratio may differ significantly. Furthermore, all swirl ratio definitions presented in this section focus on the similarity between circumferential velocity components. Therefore, no conclusion can be drawn regarding the similarity of radial and vertical velocity components.

3.1.4. The effect of the simulator’s geometry on the surface pressure field (*T1*)

Figures 4 illustrates surface pressure distributions that arise as a result of the two flow fields investigated in *S1* and *M1* for S = 0.30 and S = 0.69, respectively. In general, it can be observed that surface pressure distributions obtained for S = 0.30 (Figure 4a) increase at a faster rate from the vortex centre towards larger radial distances compared to S = 0.69 (Figure 4b). Despite the suggested central downdraft for S = 0.69 in *S1* and *M1*, the surface pressure distribution of the corresponding vortex does not show the expected two-celled vortex structure near the simulator’s centre. A potential reason for this could be that the effect of the downdraft on surface pressure measurements is too small to be captured compared to the effect of the circumferential velocity component.

Figure 4a highlights that despite of the observed flow field differences between vortices simulated in *S1* and *M1* for S = 0.30, surface pressure distributions are in good agreement and small differences lie within the experimental uncertainty. The same applies for surface pressure distributions of the larger swirl ratio for radial distances > $|0.2r/D_3|$ (Figure 4b). However, around the vortex centre, a pressure deficit which is smaller by about $0.5\delta p$ is observed in *M1* compared to *S1* ($\delta p = \left|(p(r,z=0)/p_{ref})_{S1} - (p(r,z=0)/p_{ref})_{M1}\right|$).

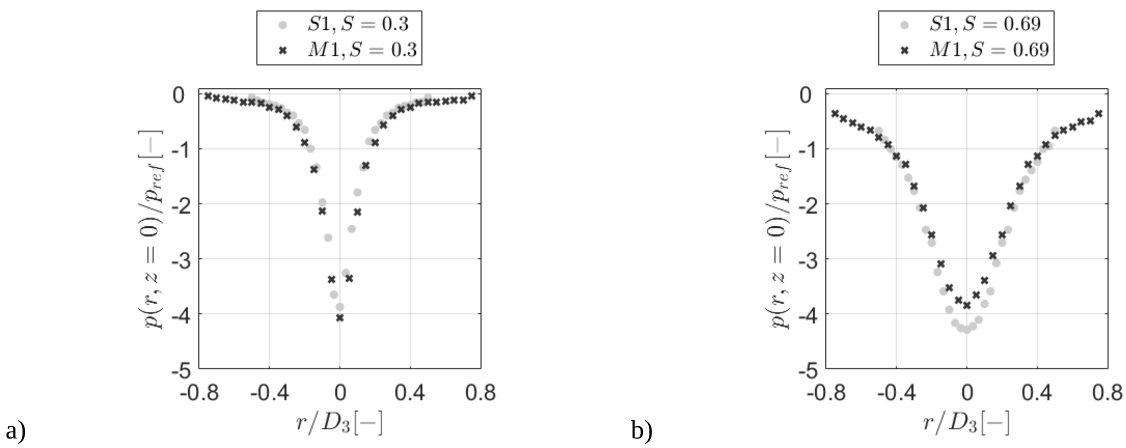

Fig. 4 Mean surface pressure distributions measured in *S1* and *M1* for S = 0.30 (a) and S = 0.69 (b)

3.2. SIMULATIONS IN S1, S2 AND S3

3.2.1 The effect of the convection chamber height on the flow field (*T2*)

In this section, the effect of changing the convection chamber height (H_2) in the small generator (whilst keeping other geometric parameters and the swirl ratio defined in equation (6) constant) is investigated.

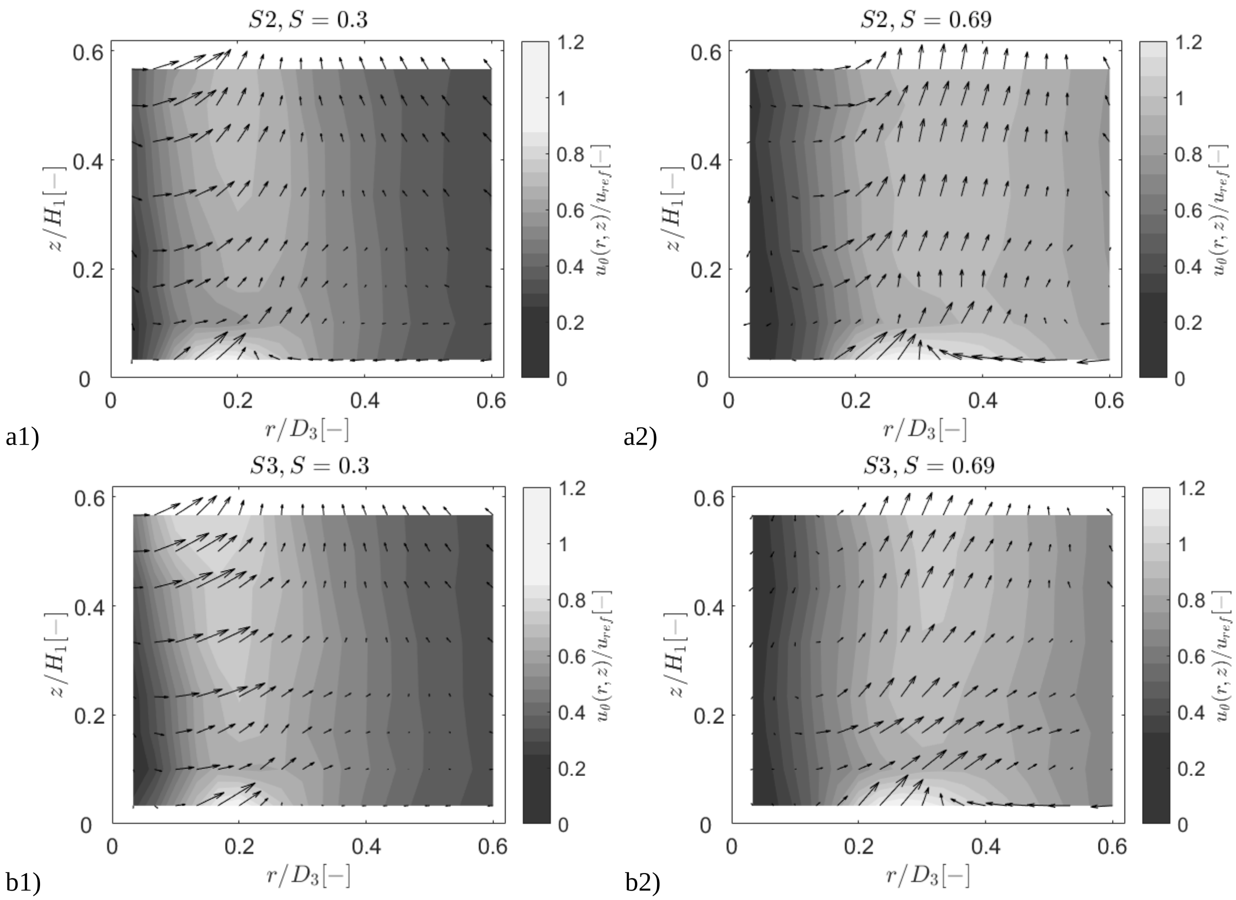

Fig. 5 Mean 3-D velocity fields in *S2* and *S3* for *S* = 0.30 and *S* = 0.69. The normalised circumferential velocity component is shown as contour and the 2-D vector field indicates the vector based on the radial and vertical velocity component.

The 3-D velocity fields obtained in *S2* (where the convection chamber height is reduced by ~38%) and *S3* (where the convection chamber height is reduced by ~75%) for both swirl ratios are shown in figure 5. Also, for those simulations a number of similarities can be highlighted. For all simulations conducted in *S2* and *S3*, radial outflow dominates the vortex core, which feeds into an updraft at a radial distance approximately equal to the corresponding vortex core. This flow behaviour appears to become more distinct with decreasing H_2, irrespective of the swirl ratio. In both simulators (*S2* and *S3*) for the lower swirl ratio (*S* = 0.30) the core radius is approximately defined at r/D_3 = 0.2. For the larger swirl ratio (*S* = 0.69) the vortex core size increases to a normalised radial distance equal to approximately r/D_3 = 0.3 (Figure 5a2 and 5b2). Furthermore, the relatively strong radial inflow close to the surface up to the position where the overall circumferential velocity maximum occurs (shown in figure 2a and 2b) appears to weaken with decreasing H_2 (Figure 5). For *S* = 0.30, the strong radial outflow and updraft observed in the vortex core of *S2* and *S3* suggests that the downdraft in *S1*, which seems to terminate aloft a stagnation point at a normalised height of approximately z/H_1 = 0.3 (Figure 2a), lowers and reaches the surface of simulator *S2* and *S3* (Figure 5a and 5c). The overall flow structure for all simulations for the larger swirl ratio suggests a vortex structure similar to what might be expected in a two-celled vortex (Figure 2b, 5b and 5d). The radial outflow inside the vortex core obtained in *S1*, *S2* and *S3* suggests a central downdraft.

For more details, differences between circumferential, radial and vertical velocity components at equal relative heights (z/H_1) in the simulators are shown in figure 6. Table 6 provides an overview of heights investigated.

Table 6: Absolute (z) and relative (z/H_1) heights for the comparison of flow fields simulated *S1*, *S2* and *S3* for S = 0.30 and S = 0.69

	S1	*S2*	*S3*
z_1 [m]	*0.01*	*0.01*	*0.01*
z_2 [m]	*0.15*	*0.15*	*0.15*
z_1/H_1	*0.03*	*0.03*	*0.03*
z_2/H_1	*0.50*	*0.50*	*0.50*

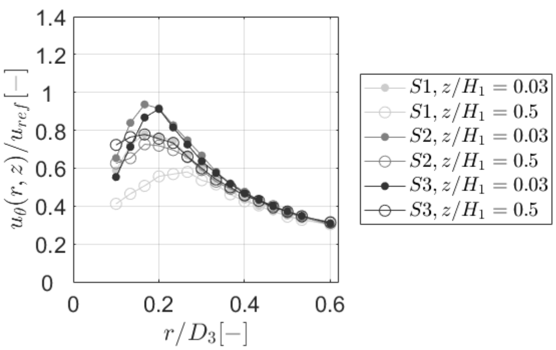

a1)

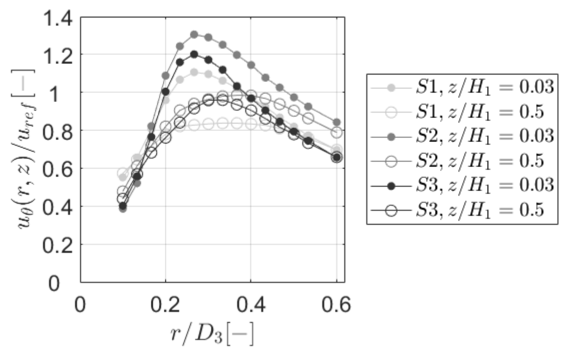

a2)

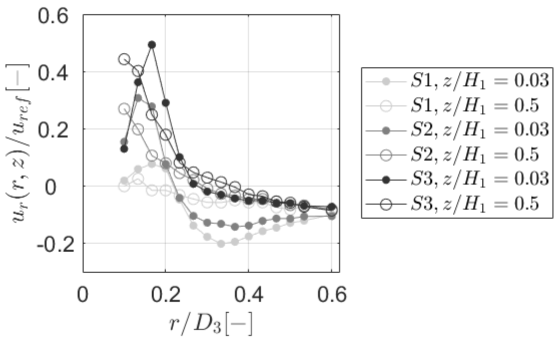

b1)

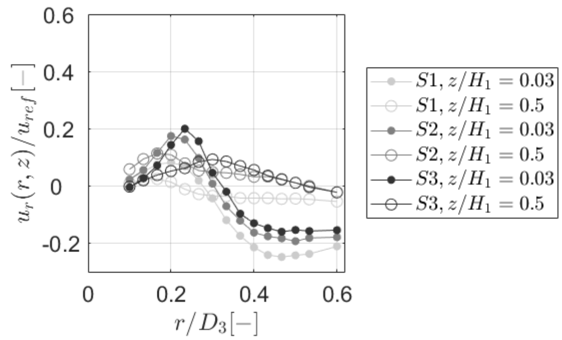

b2)

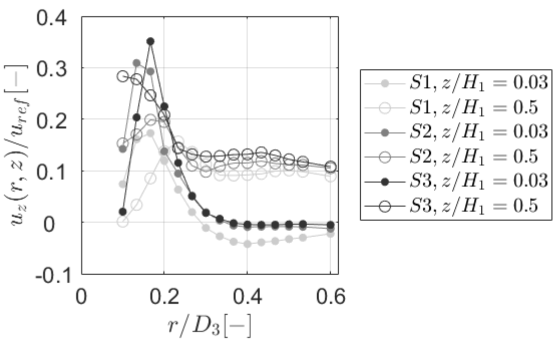

c1)

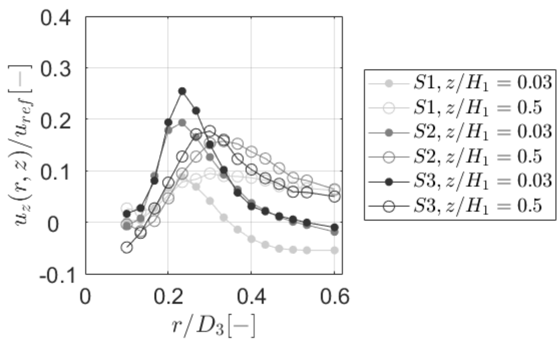

c2)

Fig. 6 Radial profile of circumferential (a), radial (b) and vertical (c) velocity components obtained in *S1*, *S2* and *S3* for *S* = 0.30 (1) and *S* = 0.69 (2) at the corresponding relative heights (z/H_1)

Figure 6a1 illustrates that circumferential velocity components obtained for *S* = 0.30 differ significantly at radial distances < 0.2 r/D_3 (Figure 6a1). Differences of about $0.3\delta u_\theta$ can be observed between vortices simulated in *S1* and *S3* at z/H_1 = 0.5. For S = 0.69 (Figure 6a2), the radial profiles of circumferential velocity components reveal differences of up to $0.2\delta u_\theta$ and $0.1\delta u_\theta$ around the region of maximum circumferential velocities for z/H_1 = 0.5 and z/H_1 = 0.03, respectively.

Differences larger than the experimental uncertainty are also found for radial velocity components (Figures 6b1 and 6b2). For S = 0.30, the radial outflow at radial distances < 0.2 r/D_3 increases significantly with decreasing H_2 (Figure 6b1). Differences of up to $0.3\delta u_r$ are found when comparing *S1* with *S2*, and a comparison between *S1* with *S3* reveals differences of approximately $0.4\delta u_r$. In addition, at r/D_3 = 0.3, a decrease in radial inflow can be observed with decreasing H_2 at the lower height (z/H_1 = 0.03). For the larger swirl ratio (S = 0.69, Figure 6b2), a reduction of H_2 by 75% seems to cause differences of about $0.2\delta u_r$. Although, differences between the flow fields of the lower swirl ratio seem to be more distinct, a similar trend can perhaps be inferred for radial velocity components of the larger swirl ratio.

Figures 6c1 and 6c2 illustrate that the vertical updraft around the corresponding vortex core region intensifies with decreasing H_2 for both swirl ratios. For the lower swirl ratio (S = 0.30), this causes differences of up to $0.15\delta u_z$ between *S1* and *S2*, and up to $0.3\delta u_z$ between *S1* and *S3* at z/H_1 = 0.5 and r/D_3 = 0.1 (Figures 6c1). For the larger swirl ratio, differences are more distinct at the lower height (Figure 6c2). In this case, differences of about $0.1\delta u_z$ and $0.15\delta u_z$ are found when comparing results obtained at r/D_3 = 0.25 in *S1* to *S2* and *S3*, respectively.

3.2.2 The effect of the convection chamber height on the surface pressure field (*T2*)

The radial profiles of surface pressures measured in *S1*, *S2* and *S3* for *S* = 0.30 (a) and *S* = 0.69 (b) are presented in figure 7. Figure 7 reveals that despite of flow field differences highlighted for S = 0.30, the surface pressure distributions illustrated in figure 7a seem to be largely unaffected by the changes of H_2. The surface pressure distribution of the larger swirl ratio on the other hand (Figure 7b) shows significant differences for most radial distances. In particular around the vortex centre, differences of about $1.5\delta p$ are illustrated between surface pressure distributions measured in *S2* and *S3*.

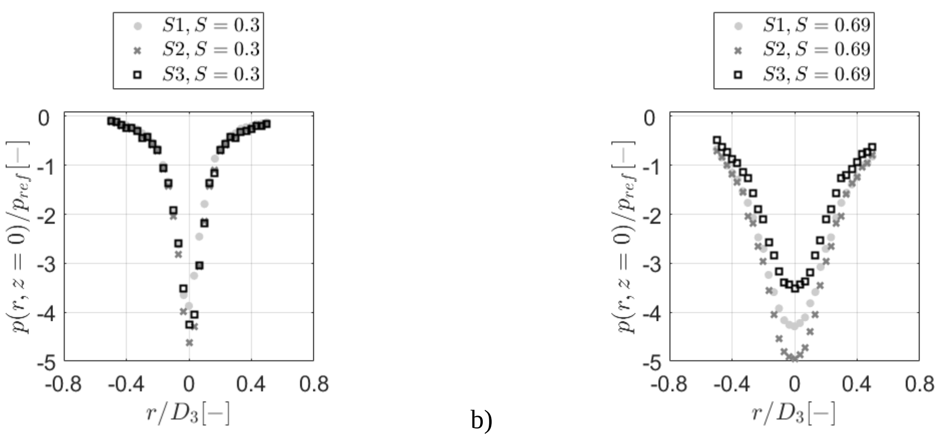

a) b)

Fig. 7 Mean surface pressure distributions obtained in *S1*, *S2* and *S3* for *S* = 0.30 (a) and *S* = 0.69 (b)

4. CONCLUDING REMARKS

Based on this analysis, the following main conclusions can be drawn:

- Time averaged velocity and surface pressure data have been presented and illustrate (in keeping with previous work) that the swirl ratio has an effect on the vortex size, pressure distribution and velocity characteristics.

- Velocity and surface pressure characteristics of vortices generated in simulators of different geometry and scale, but with swirl ratio and aspect ratio parity can differ significantly. Based on this, it is suggested that ensuring aspect ratio and swirl ratio parity between different simulators is not sufficient to generate similar vortices with similar velocity and surface pressure characteristics, i.e. not surprisingly, all boundary conditions govern the flow.

- Flow field and surface pressure characteristics of tornado-like vortices appear also to be a function of the convection chamber height.

- It was found that the effect of the simulator's geometry on the flow and surface pressure field can be swirl ratio dependent.

- It has been shown that an agreement between surface pressure distributions is not sufficient to conclude flow field similarity.

Compliance with Ethical Standards

Conflict of Interest: The authors declare that they have no conflict of interest.

REFERENCES

1. *Solari G, Rainisio D and De Gaetano P (2017) Hybrid simulation of thunderstorm outflows and wind-excited response of structures. Meccanica 52:3197-3220. https://doi.org/10.1007/s11012-017-0718-x*

2. *Brusco S, Lerzo V and Solari G (2019) Directional response of structures to thunderstorm outflows. Meccanica:1-26. https://doi.org/10.1007/s11012-019-00986-5.*

3. *Jesson M, Lombardo FT, Sterling M, Baker CJ (2019) The physical simulation of a transient, downburst-like event – How complex does it need to be? Journal of Wind Engineering and Industrial Aerodynamics 189:135-150. https://doi.org/10.1016/j.jweia.2019.03.021*

4. *Letchford CW, Mans C, Chay MT (2002) Thunderstorms–their importance in windengineering (a case for the next generation wind tunnel). Journal of Wind Engineering and Industrial Aerodynamics 90:1415–1433. https://doi.org/10.1016/S0167-6105(02)00262-3*

5. *NOAA 2011 National Oceanic and Atmospheric Administration – U.S. Department of Commerce. https://www.ncdc.noaa.gov/sotc/tornadoes/201113. Accessed: 6 June 2018.*

6. *Hoecker WH (1960) Wind speed and air flow patterns in the Dallas tornado of April 2, 1957. Monthly Weather Review 88:167-180. https://doi.org/10.1175/1520-0493(1960)088<0167:WSAAFP>2.0.CO;2*

7. *Winn WP, Hunyady SJ, Aulich GD (1999) Pressure at the ground in a large tornado. Journal of Geophysical Research: Atmospheres 104:22067-22082. https://doi.org/10.1029/1999JD900387*

8. *Wurman J, Gill S (2000) Finescale Radar Observations of the Dimmitt, Texas (2 June 1995), Tornado. Monthly Weather Review 128:2135-2164. https://doi.org/10.1175/1520-0493(2000)128<2135:FROOTD>2.0.CO;2*

9. *Lee J, Samaras T, Young CR (2004) Pressure measurements at the ground in an F-4 tornado. The 22nd Conference on Severe Local Storms, Anonymous Hyannis, MA.*

10. *Wurman J and Alexander CR (2004) The 30 May 1998 Spencer, South Dakota, Storm. Part II: Comparison of Observed Damage and Radar-Derived Winds in the Tornadoes. Monthly Weather Review 133:97-119.*https://doi.org/10.1175/MWR-2856.1

11. *Lee WC and Wurman J (2005) Diagnosed Three-Dimensional Axisymmetric Structure of the Mulhall Tornado on 3 May 1999. Journal of the Atmospheric Sciences 62:2373-2393.* https://doi.org/10.1175/JAS3489.1

12. *Karstens CD, Samaras TM, Lee BD, Gallus Jr WA, Finley CA (2010) Near-Ground Pressure and Wind Measurements in Tornadoes. Monthly Weather Review 138:2570-2588.* https://doi.org/10.1175/2010MWR3201.1

13. *Kosiba K, Wurman J (2010) The Three-Dimensional Axisymmetric Wind Field Structure of the Spencer, South Dakota, 1998 Tornado. Journal of the Atmospheric Sciences 67:3074-3083.* https://doi.org/10.1175/2010JAS3416.1

14. *Wurman J, Kosiba K, Robinson P (2013) In Situ, Doppler Radar, and Video Observations of the Interior Structure of a Tornado and the Wind–Damage Relationship. Bulletin of the American Meteorological Society 94:835-846.* https://doi.org/10.1175/BAMS-D-12-00114.1

15. *Refan M, Hangan H, Wurman J, Kosiba K (2017) Doppler radar-derived wind field of five tornado events with application to engineering simulations. Engineering Structures 148:509-521.* https://doi.org/10.1016/j.engstruct.2017.06.068

16. *Ward NB, (1972) The Exploration of Certain Features of Tornado Dynamics Using a Laboratory Model. Journal of the Atmospheric Sciences 29:1194-1204.* https://doi.org/10.1175/1520-0469(1972)029<1194:TEOCFO>2.0.CO;2

17. *Church CR, Snow JT, Baker GL, Agee EM (1979) Characteristics of Tornado-Like Vortices as a Function of Swirl Ratio: A Laboratory Investigation. Journal of the Atmospheric Sciences 36:1755-1776.* https://doi.org/10.1175/1520-0469(1979)036<1755:COTLVA>2.0.CO;2

18. *Haan Jr FL, Sarkar PP, Gallus WA (2008) Design, construction and performance of a large tornado simulator for wind engineering applications. Engineering Structures 30:1146-1159.* https://doi.org/10.1016/j.engstruct.2007.07.010

19. *Mishra AR, James DL, Letchford CW (2008) Physical simulation of a single-celled tornado-like vortex, Part A: Flow field characterization. Journal of Wind Engineering and Industrial Aerodynamics 96:1243-1257.* https://doi.org/10.1016/j.jweia.2008.02.063

20. *Sabareesh GR, Matsui M, Tamura Y (2012) Dependence of surface pressures on a cubic building in tornado like flow on building location and ground roughness. Journal of Wind Engineering and Industrial Aerodynamics 103:50-59.* https://doi.org/10.1016/j.jweia.2012.02.011

21. *Refan M, Hangan H (2016) Characterization of tornado-like flow fields in a new model scale wind testing chamber. Journal of Wind Engineering and Industrial Aerodynamics 151:107-121.* https://doi.org/10.1016/j.jweia.2016.02.002

22. *Refan M and Hangan H (2018) Near surface experimental exploration of tornado vortices. Journal of Wind Engineering & Industrial Aerodynamics 175:120–135.* https://doi.org/10.1016/j.jweia.2018.01.042

23. *Gillmeier S, Sterling M, Hemida H, Baker CJ (2018) A reflection on analytical tornado-like vortex flow field models. Journal of Wind Engineering and Industrial Aerodynamics 174:10-27. https://doi.org/10.1016/j.jweia.2017.12.017*

24. *Tang Z, Feng C, Wu L, Zuo D, James DL (2018a) Characteristics of Tornado-Like Vortices Simulated in a Large-Scale Ward-Type Simulator. Boundary-Layer Meteorology 166:327–350. http://dx.doi.org/10.1007/s10546-017-0305-7*

25. *Davies-Jones RP (1973) The Dependence of Core Radius on Swirl Ratio in a Tornado Simulator. Journal of the Atmospheric Sciences 30:1427-1430. https://doi.org/10.1175/1520-0469(1973)030<1427:TDOCRO>2.0.CO;2*

26. *Tang Z, Zuo D, James D, Eguchi Y, Hattori Y (2018b) Effects of Aspect Ratio on Laboratory Simulation of Tornado-Like Vortices. Wind and Structures 27:111-121. http://dx.doi.org/10.12989/was.2018.27.2.111*

27. *Wan CA and Chang CC (1972) Measurement of the Velocity Field in a Simulated Tornado-Like Vortex Using a Three-Dimensional Velocity Probe. Journal of the Atmospheric Sciences 29:116-127. https://doi.org/10.1175/1520-0469(1972)029<0116:MOTVFI>2.0.CO;2*

28. *Jischke MC and Parang M (1974) Properties of Simulated Tornado-Like Vortices. Journal of the Atmospheric Science 11:506–512. https://doi.org/10.1175/1520-0469(1974)031%3C0506:POSTLV%3E2.0.CO;2*

29. *Zhang W and Sarkar PP (2012) Near-ground tornado-like vortex structure resolved by particle image velocimetry (PIV). Exp. Fluids 52:479-493. https://doi.org/10.1007/s00348-011-1229-5*

30. *Hashemi-Tari P, Gurka R, Hangan H (2010) Experimental investigation of tornado-like vortex dynamics with swirl ratio: The mean and turbulent flow fields. Journal of Wind Engineering and Industrial Aerodynamics 98:936-944. https://doi.org/10.1016/j.jweia.2010.10.001*

31. *Gillmeier S., Sterling, M., Baker, C., 2017. An analysis of non-stationary processes in tornado-like vortices. International Workshop on Physical Modelling of Flow and Dispersion Phenomena. France*

32. *Church CR, Snow JT, Agee, EM (1977) Tornado Vortex Simulation at Purdue University. American Metrological Society 58:900–908. https://doi.org/10.1175/1520-0477(1977)058<0900:TVSAPU>2.0.CO;2*